Tunable charge density wave in TiS_3 nanoribbons*

Ce Huang(黄策)[1,2], Enze Zhang(张恩泽)[1,2], Xiang Yuan(袁翔)[1,2], Weiyi Wang(王伟懿)[1,2], Yanwen Liu(刘彦闻)[1,2], Cheng Zhang(张成)[1,2], Jiwei Ling(凌霁玮)[1,2], Shanshan Liu(刘姗姗)[1,2], and Faxian Xiu(修发贤)[1,2,3,†]

[1] *State Key Laboratory of Surface Physics and Department of Physics, Fudan University, Shanghai* 200433, *China*
[2] *Institute for Nanoelectronic Devices and Quantum Computing, Fudan University, Shanghai* 200433, *China*
[3] *Collaborative Innovation Center of Advanced Microstructures, Nanjing* 210093 *China*

(Received 29 April 2017; revised manuscript received 4 May 2017; published online 20 May 2017)

Recently, modifications of charge density wave (CDW) in two-dimensional (2D) show intriguing properties in quasi-2D materials such as layered transition metal dichalcogenides (TMDCs). Optical, electrical transport measurements and scanning tunneling microscopy uncover the enormous difference on the many-body states when the thickness is reduced down to monolayer. However, the CDW in quasi-one-dimensional (1D) materials like transition metal trichalcogenides (TMTCs) is yet to be explored in low dimension whose mechanism is likely distinct from their quasi-2D counterparts. Here, we report a systematic study on the CDW properties of titanium trisulfide (TiS_3). Two phase transition temperatures were observed to decrease from 53 K (103 K) to 46 K (85 K) for the bulk and $<$ 15-nm thick nanoribbon, respectively, which arises from the increased fluctuation effect across the chain in the nanoribbon structure, thereby destroying the CDW coherence. It also suggests a strong anisotropy of CDW states in quasi-1D TMTCs which is different from that in TMDCs. Remarkably, by using back gate of -30 V $\sim$ 70 V in 15-nm device, we can tune the second transition temperature from 110 K (at -30 V) to 93 K (at 70 V) owing to the altered electron concentration. Finally, the optical approach through the impinging of laser beams on the sample surface is exploited to manipulate the CDW transition, where the melting of the CDW states shows a strong dependence on the excitation energy. Our results demonstrate TiS_3 as a promising quasi-1D CDW material and open up a new window for the study of collective phases in TMTCs.

Keywords: TiS_3, two-dimensional material, charge density wave, phase transition

PACS: 73.22.Pr **DOI:** 10.1088/1674-1056/26/6/067302

1. Introduction

Periodic modulations of electron density from electron–phonon interactions lead to a novel type of ground state called charge density wave (CDW).[1] A great deal of materials such as layered transition metal dichalcogenides (TMDCs) and transition metal trichalcogenides (TMTCs) have been found to possess the CDW states.[1,2] Recently, these interesting states show unexpected and exotic properties when approaching the 2D limit. For example, with the thickness decreasing,[3] a commensurate CDW state completely disappears in TaS_2; and the transition temperature can be drastically enhanced in monolayer $NbSe_2$ and $TiSe_2$.[4–7] More interestingly, the quantum critical behavior may exist in 2D TaS_2 and other correlated systems[8,9] as the reduced dimensionality can strengthen Peierls instability, electron–phonon interactions, and the fluctuation effect.[1,7] Therefore, it is indispensable to investigate the effect of the dimensionality on the CDW states and uncover the intrinsic mechanism.

Like TMDCs, many bulk TMTCs exhibit layered structures with interlayer van der Waals interactions.[10–12] As a typical TMTC, MX_3-type crystals (M = Ti, Zr, Hf, Ta, Nb; X = S, Se, Te) are quasi-1D materials, some of which possess charge density waves in the bulk form. And these states emerge and slide along the direction of metal-atom chains unlike in TMDC materials where the various CDW states are developed by several-atoms-clusters in 2D layers.[13,14] For instance, two phase transitions at 144 K and 59 K in $NbSe_3$ are the consequence of three structurally different chains.[15] Monoclinic TaS_3 has two types of chains which induce CDW transitions at 240 K and 160 K.[16] Importantly, the low dimensionality may exert strong effects on those chain-like quasi-1D materials due to the different crystal structures. Each CDW transition can be variously affected with the change of device scale along different crystal orientations, thus giving rise to an evident anisotropy. However, limited works have been reported on the CDW states in quasi-1D TMTC materials when the dimensionality is reduced to two dimensions.

TiS_3, as one of the semiconducting TMTCs, shows extremely excellent optical properties.[17–21] Strong anisotropy from electric transport measurements represents 30% of increase over the black phosphorus.[19,22] The bulk crystals have phase transitions at 120, 60, and 17 K through quasi-

*Project supported by the National Young 1000-Talent Plan and the National Natural Science Foundation of China (Grant Nos. 61322407, 11474058, and 61674040).

†Corresponding author. E-mail: Faxian@fudan.edu.cn

© 2017 Chinese Physical Society and IOP Publishing Ltd

1D transport.[23–26] with the first two along the perpendicular chains. We anticipate that the nanoribbon structure can have structural fluctuations in horizontal and perpendicular directions that lead to anisotropic CDW behavior upon external electrical gating. However, to date such studies remain lacking.

Here, we report the properties of exfoliated few-layer TiS_3 nanoribbons and find only two phase transitions at 46 K (T_{c1}) and 85 K (T_{c2}) in stark contrast to the three in thick TiS_3 at 29, 53, and 103 K. T_{c2} can be tuned by the back-gate voltage because of the variable carrier concentration whereas T_{c1} does not show an evident change owing to its robustness to the structural fluctuations. Our transport experiments clearly exhibit a strong anisotropy of CDW states in TiS_3. We also reveal the light-induced melting of charge density wave under 633-nm laser illumination. When the laser intensity exceeds 10 μW, both two transitions disappear. Moreover, a low illumination intensity of 0.02 μW by a 532-nm laser can readily destroy the CDW states.

2. Methods

2.1. Growth and characterizations of TiS_3 nanoribbons

TiS_3 was synthetized by sulfuration of Ti using chemical vapor transport (CVT) method.[13] 0.23-g titanium powder and 0.6-g sulfur powder were sealed in an evacuated quartz ampule. The ampule was placed in a tube furnace, where it was heated up to 500 °C for 1 day, then kept at 500 °C for 1 day for sulfuration. The cooling process took place in ambient conditions. Sulfur vapor pressure at 500 °C was around 4 bars (1 bar = 10^5 Pa).

Raman spectroscopy measurements were performed at a self-built Raman system with a laser wavelength of 532 nm. The diameter of focused laser spot is less than 2 μm when using a 100-μm pin hole.

2.2. Device fabrication and transport measurements

The electrodes of the device were fabricated by EBL using MMA/PMMA bilayer polymer. Cr/Au (5 nm/100 nm) electrodes were deposited by sputtering. The temperature-dependent transport measurements of the 4-probe device were carried out in a Physical Property Measurement System (PPMS) system (Quantum design) using an Agilent 2912.

2.3. Light-induced transport measurement

The light-induced transport measurements were carried out in an optical dry cryogenic system (Oxford Instruments, OptistatDry BL4).

3. Results

Bulk TiS_3 crystals were synthesized via chemical vapor transport (CVT) method (sulphuration of titanium powder).[17]

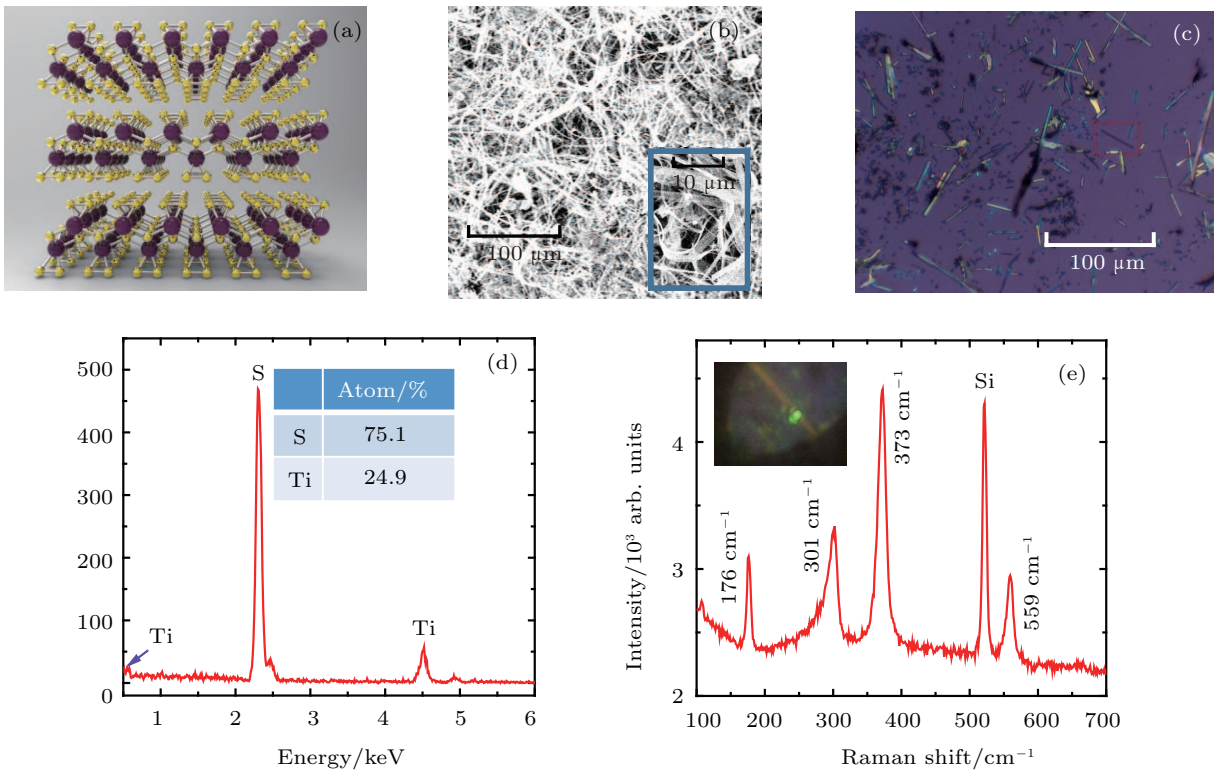


Fig. 1. (color online) Synthesis and characterizations of TiS_3 nanoribbons. (a) The TiS_3 crystal structure. Ti atoms are covalently bonded to six S atoms forming triangular prisms which are stacked to make chains. (b) The optical microscopy image of TiS_3 nanoribbons on an SiO_2/Si substrate. (c) The SEM image of TiS_3 nanoribbons. Inset: single TiS_3 nanoribbon. (d) The EDX spectrum of TiS_3 nanoribbons with the atomic ratio of Ti/S of 1:3. (e) The Raman spectrum of the individual TiS_3 nanoribbon on SiO_2/Si substrate at room temperature using a 532-nm laser source.

Figure 1(a) shows a layered structure of TiS_3; parallel chains of triangular prisms which are held by van der Waals forces constitute sheets. The parallel chains are responsible for the quasi-1D nature of the material which leads to charge density waves. Each sheet is formed by two titanium layers and four sulfide layers. The as-grown TiS_3 naturally develops groups of black needle-like bulk crystals. Figure 1(b) shows one of the exfoliated TiS_3 samples transferred onto SiO_2(285 nm)/Si substrate with a number of nanoribbons. Figure 1(c) shows a scanning electron microscopy (SEM) image, where both bulk crystals and thin nanoribbons can be identified. The purple one in the red rectangle is a thin nanoribbon with a thickness of 7 nm $\sim$ 8 nm. To identify the composition of sample, energy dispersive x-ray spectroscopy (EDX) has been carried out. Figure 1(d) displays the EDX results of the as-grown samples. More than five positions have been randomly picked and measured, all of which show clear peaks of Ti and S with the total error less than 0.5%. The atomic ratio of Ti and S is nearly Ti:S=1:3, indicating a correct composition of TiS_3. We further carried out Raman spectroscopy to explore the phonon characteristics of materials and identify the chemical bond. Figure 1(e) displays the Raman spectrum of an isolated nanoribbon thicker than 50 nm; the optical image of the sample is shown in the inset under 532-nm laser illumination. While the peak at ~ 520 cm^{-1} is due to Raman mode of silicon substrate, the other four peaks located at 176 cm^{-1}, 301 cm^{-1}, 373 cm^{-1}, and 559 cm^{-1} correspond to A_g-type Raman modes of the TiS_3 which are in good agreement with the bulk crystals. Besides, a previous study reports the observation of the 373 cm^{-1} peak which has the highest intensity along b axis in nanoribbons,[27] which is consistent with our results.

In order to study the CDW properties, four-terminal devices with Cr/Au (5 nm/100 nm) electrodes were fabricated along the nanoribbon chain direction, i.e., the b axis, by standard e-beam lithography, metal evaporation, and lift-off process. Temperature-dependent resistance (R–T) is measured from room temperature down to 10 K as shown in Fig. 2(a). The inset displays the device image by a conventional optical microscope. The length of the sample is around 20 μm and the width is 2 μm. The thickness of the nanoribbon is determined to be 50 nm $\sim$ 60 nm, which is relatively thick. The resistivity measured at 300 K has a value of $\rho = 0.4\ \Omega\cdot$cm^{-1} in good agreement with the previously-reported bulk results.[28] The R–T curves in our experiments are all measured in the cooling process to eliminate the hysteresis induced by the system. As the temperature cools down, the resistance shows several broad anomaly features. In order to clearly identify the transition temperatures, we adopted the widely-used derivative method and plotted $\mathrm{d}\ln R/\mathrm{d}(1/R)$ against the temperature. It is known that near the transition temperature, the conductivity can be extracted by

$$\sigma = \mu N_{\mathrm{e}}\left[1 - \frac{1.74\pi}{4T_{\mathrm{c}}^2}(T_{\mathrm{c}} - T)^2\right]$$

based on the mean-field theory, where μ is the mobility and N_{e} is the density of states.[16] When $T < T_{\mathrm{c}}$, the temperature derivative of the resistivity is approximately given by

$$\frac{\mathrm{d}\rho}{\mathrm{d}(1/T)} \approx \frac{1.74\pi}{2\mu N_{\mathrm{c}} T_{\mathrm{c}}^2}\frac{1}{(T_{\mathrm{c}} - T)^{1/2}}.$$

Consequently, the derivative $\mathrm{d}\ln\rho/\mathrm{d}(1/T)$ has a cusp singularity at transition temperature. Here, we use the maxima from the derivative curve.[29] to estimate the transition temperature of 29, 53, and 103 K in the 50 nm $\sim$ 60 nm-thick nanoribbon, which are similar to that of the bulk crystals.[23] Instead of showing a cusp, one observes a broadened maximum, which is consequence of fluctuations caused by the 2D dimensionality. At the same time, quasi-1D systems always induce nonlinear conductivity due to the sliding or creeping of the CDW states.[30] And the current–voltage (I–V) curves follow the power law behavior $I \propto V^{\alpha}$ in CDW systems (along the chains) at low temperatures. Indeed, the I–V curve at 10 K exhibits a voltage-dependent conductivity whereas at 130 K it becomes linear with a constant conductivity. Figure 2(b) summarizes all I–V curves in the temperature range of 10 K to 130 K where a nonlinear behavior is exclusively observed. However, owing to the possible contribution from the Schottky barrier which is observed in monolayer MoS_2 using four-point probe measurement, the exact onset of the CDW transition remains elusive.[31] We note that the four-probe method is unsuitable if the Schottky behavior occurs between the metallic contact and the sample where the Schottky barrier induces a large contact resistance causing inaccuracy of sample resistance.[32,33] Since the nanoribbon is thick enough, the drain–source current I_{ds} can be defined by three-dimensional (3D) thermionic emission equation[34]

$$I_{\mathrm{ds}} = AST^2\exp\left[-\frac{q}{k_{\mathrm{B}}T}\left(\Phi_{\mathrm{B}} - \frac{V_{\mathrm{ds}}}{n}\right)\right],$$

where A is the Richardson constant, n is the ideality factor. The fitting results show a Schottky barrier Φ_{B} of 42.3 meV (see Fig. S1 in the supplementary information in Appendix A). Thus, our I–V curves consist of contributions from both quasi-1D CDW and Schottky barrier. When the voltage is larger than 0.4 V, $\ln I_{\mathrm{ds}}$ is proportional to V, matching the thermionic emission model (Fig. S1(a), and the current induced by Schottky barrier at low voltage is much smaller than that from the quasi-1D transport. Therefore, at low voltage, the quasi-1D transport dominates while the Schottky barrier plays important roles at the high-voltage regime. When the voltage is lower than the threshold, the electrons cannot be excited across the CDW gap in a two-fluid model.[1] The current can be written as $I_{\mathrm{tot}} = I_{\mathrm{n}} + I_{\mathrm{CDW}}$, where the subscripts n and CDW refer to

the current carried by the uncondensed and condensed electrons. The former has an Ohmic contribution and the latter has a nonlinear response. For CDW materials, the threshold field E_T is around few millivolt per micron,[1] which is much lower than that in the fitting region of Fig. 2(b). Moreover, no threshold field is observed in nonlinear transport measurements in bulk TiS_3 in the high temperature region,[23] unlike the characteristics in very thin $NbSe_3$ samples with disorders.[35] At 4.2 K, the threshold field E_T is reported to be 6 V/cm.[36] Therefore, at a specific temperature, the *I*–*V* curves have two linear parts as shown in the inset of Fig. 2(c); the blue region is dominated by the quasi-1D CDW transport and the red regime corresponds to the Schottky barrier. We fit both the two regions by using the power law $I \propto V^{\alpha}$ at different temperatures; the resultant temperature-dependent parameter α is illustrated in Fig. 2(c). It can be seen that α becomes larger than 1 as the temperature goes below 110 K and a sharp increase occurs at about 60 K.

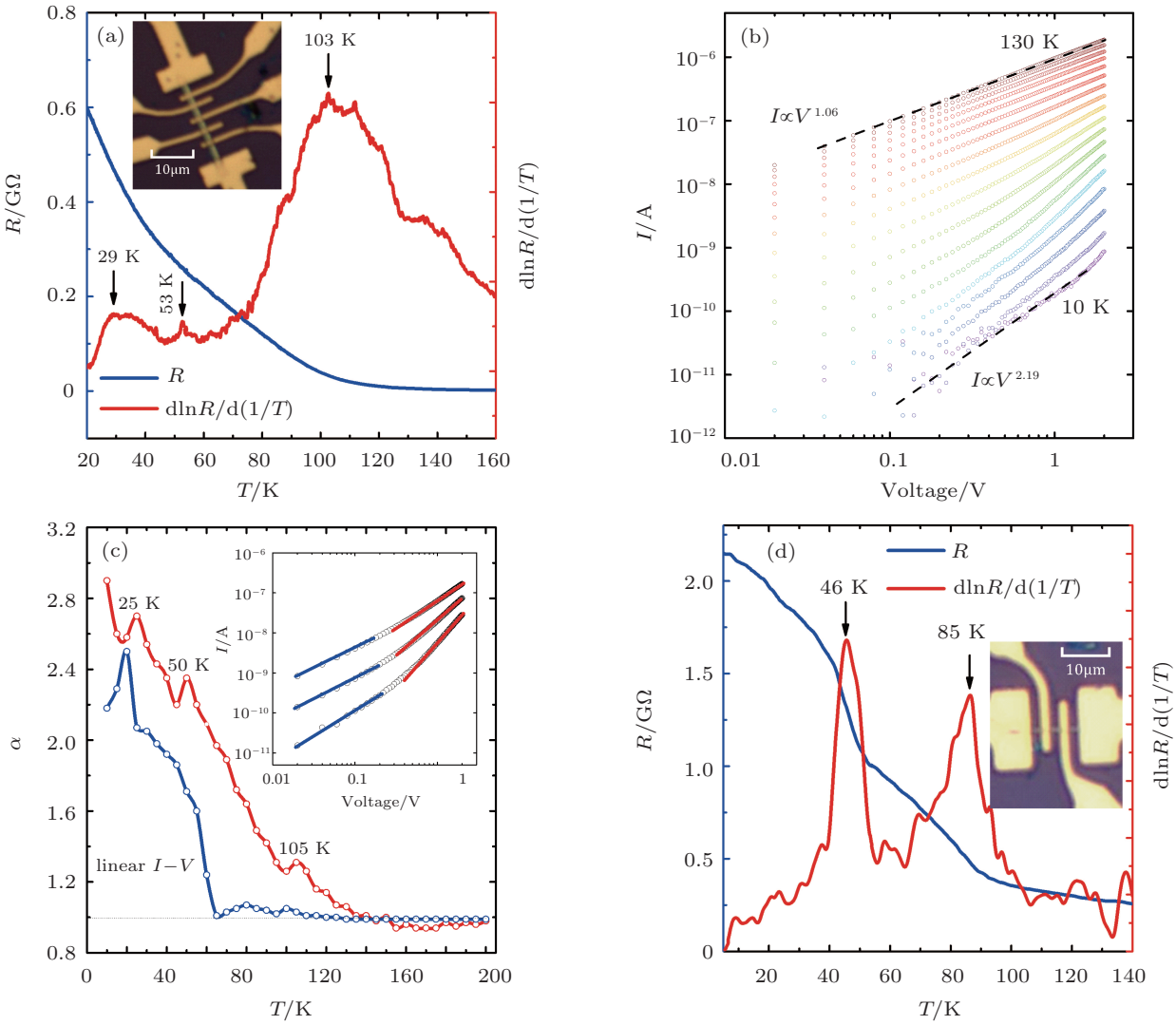


Fig. 2. (color online) CDW transitions in a 50 nm ∼ 60 nm thick and 15-nm thin TiS_3 nanoribbon. (a) The temperature dependence of the resistance and the logarithmic derivative $\mathrm{d}\ln R/\mathrm{d}(1/T)$. The source–drain current $I_{ds} = 5$ nA. Three CDW transitions are evident at 29, 53, and 103 K. Inset: optical microscopy image of the 50 nm–60 nm TiS3 FET. (b) I_{ds}–V_{ds} curves of the thick TiS3 nanoribbon at different temperatures. (c) The temperature dependence of parameter α using different fitting region. The red curve is fitted at $V > 0.4$ V, while the blue one is at $V < 0.4$ V. The inset shows the two fitting regions. (d) Temperature dependence of the resistance and the logarithmic derivative $\mathrm{d}\ln R/\mathrm{d}(1/T)$ in a device whose thickness is lower than 15 nm. The source drain current $I_{ds} = 2.5$ nA. Unlike the thick nanoribbon, two CDW transitions appear at 46 K and 85 K. Inset: optical image of the FET device.

The phase transitions at 53 K and 103 K can be explained by the formation of two charge density waves in disordered quasi-1D system. It was found that below 110 K, a CDW state develops in the direction across the chains, like $ZrTe_3$, while the other CDW forms along the chains below 60 K.[23] Our narrow TiS_3 nanoribbon increases the fluctuation in the direction across the chains, thus weakening the CDW, which also explains the weak non-linear transport after the first CDW state at 110 K. When the temperature is below 25 K, the noise at low voltage becomes ignorable; correspondingly the fitting parameter α has large errors to be analyzed. As the voltage becomes larger, the Schottky barrier turns to be prominent (the red curve). Below 130 K, the *I*–*V* curve turns to be nonlinear, and α gets larger with the temperature reduced, but three

peaks clearly show up with two of which corresponding to the aforementioned two CDW states. The transition at 25 K, however, is still unknown and needs further investigation. The transition temperatures from the quasi-1D transport analysis and $\mathrm{d}\ln R/\mathrm{d}(1/T)$ derivative curve are quite similar, which also confirms the three CDW phase transitions.

Next, we focus on the thinner nanoribbons. The fabrication method is the same as before, but the sample thickness is reduced to < 15 nm as displayed in the inset of Fig. 2(d). Note that experimentally it is challenging to reach monolayer TiS_3 nanoribbon because of the 1D chain structure and the subsequent electric measurements are difficult owing to the extremely large resistance when approaching the atomic thickness. The R–T curve shows anomaly peaks at 46 K and 85 K (the blue curve), which correspond to the two peaks in the derivative curve (in red). The third transition cannot be observed in transport measurements for which the underlying mechanism is not clear yet. We note that the carrier density can strongly affect the CDW phase.[16,37] Compared with the thick device, in the thin nanoribbons we find a rapid diminishment of the two transition temperatures. We provide two reasons to explain this behavior as follows. First, the scattering mechanism in TiS_3 is dominated by charge impurities at low temperatures (see Fig. S2 in Appendix A). The phase transition is greatly suppressed by impurities in quasi-2D or 1D CDW materials.[16] Non-isoelectronic impurities can induce potentials which lead to changes of the phase of the condensate, destroy long-range CDW order and lead to a finite phase–phase correlation length l_0.[38,39] Second, lowering the dimensionality of a system usually tends to reduce the phase space available for the phase parameter φ to adapt to imperfections, and consequently it suppresses the long-range order and lowers the transition temperature T_{CDW}.[16] Moreover, the Coulombic interaction can modulate transport properties in two dimensions.[40] With the thickness decreased, the interaction between the SiO_2/Si substrate and TiS_3 nanoribbon gradually dominates which can also jeopardize the CDW coherence. The size effect of CDW transition temperature can be described by empirical formula[41]

$$T_{\mathrm{c}} = T_{\mathrm{c0}}\left(1 - \frac{d_0}{d}\right) - \Delta T,$$

where T_{c0} is the bulk CDW transition temperature, d_0 is the critical thickness at which the CDW transition vanishes, ΔT is a temperature correction term. Alternatively, we think that the second CDW transition is more stable in the bulk or nanosheet but not in nanoribbon (chains) because T_{c2} is in the direction across the chains. In other words, the interlayer coupling is unfavorable for the second CDW state. The device in Fig. 3(b) has a phase transition at 40 K and 100 K, which is different from the device in Fig. 3(a). This may be due to the different thicknesses, impurities, and electron concentrations. Therefore, at large gate voltage the T_{c2} decreases. The transition temperature in TiS_3 nanoribbon shows opposite thickness-dependence trend with quasi-2D TMDCs ($NbSe_2$, $TiSe_2$) which will help us to better understand the relation between Peierls instabilities and fluctuation effects.[7,42]

In bulk materials, the doping and high pressure can modulate the carrier density, for instance, to enhance the superconductivity in Cu-doped $TiSe_2$.[43] In quasi-2D materials, the electric-field effect is much more convenient than these two methods: a gate voltage can induce a large number of electrons (holes) into the system so that CDW can be easily tuned.[3,37] Here, we use a back-gate voltage to tune the phase transitions in 15-nm thick nanoribbon. Figure 3(a) illustrates a set of R–T curves at gate voltage ranging from -30 V to 70 V using a constant source–drain current of 1.5 nA. At 40 K, the resistance changes from 2.6 GΩ to 0.07 GΩ. From $V_{\mathrm{g}} = -30$ V to $V_{\mathrm{g}} = 70$ V, a peak can be clearly identified near the first transition temperature (Fig. 3(a)). The semiconducting phase converting to be metallic looks more evident when we use logarithmic coordinates as demonstrated in the inset. It is possible that the large CDW conduction modulation is due to changes in CDW pinning arising from gate–voltage-induced variations in the CDW gap which was also observed in semiconducting quasi-1D material TaS_3.[44] Likewise, figure 3(b) displays the derivative curves to ensure the extraction of the transition temperature. Apparently, two peaks are shifted as a function of the gate voltage. The gate–voltage dependence of conductance at 160 K is displayed in Fig. S2(b). At $V_{\mathrm{g}} = -80$ V, the conductance tends to be zero and the extracted field-effect mobility and on/off ratio are 0.8 $\mathrm{cm}^2 \cdot \mathrm{V}^{-1} \cdot \mathrm{s}^{-1}$ and ~ 25, respectively (More information is available in Figs. S2 and S3 in Appendix A). Systematic T_{c} changes under different gate voltages are summarized in Fig. 3(c). For the first CDW transition, the critical transition temperature does not vary much and it positions at around 40 K. On the contrary, T_{c2} is identified to be 110 K when $V_{\mathrm{g}} = -30$ V and reduced to 93 K at $V_{\mathrm{g}} = 70$ V and in the whole gate region T_{c2} has negative dependence with the value of gate voltage. It can be naturally explained by the fact that the increase of the electron density at positive voltages suppresses T_{c2}, which is also supported by a similar behavior occurring in 1T-$TiSe_2$ and TaS_2.[3,37] Specifically, a large electron density may enhance CDW phase fluctuations, strengthen disorders, and thus ultimately destroy a long-range CDW coherence. More electrons tend to be excited across the gap, the periodic structure of charge density becomes unstable and much lower temperature is needed to reduce the thermal excitation and keep the density wave. This is commonly observed in quasi-1D and quasi-2D systems.[16] In contrast, T_{c1}

decreases a little at larger V_g; this is presumably caused by its robustness to the fluctuations because of the ribbon structure in which the CDW forms along the chains. However, for the thick nanoribbon sample, the gate cannot tune it well in a sharp contrast to the thin one, as shown in Fig. S4 in the supplementary information (Appendix A).

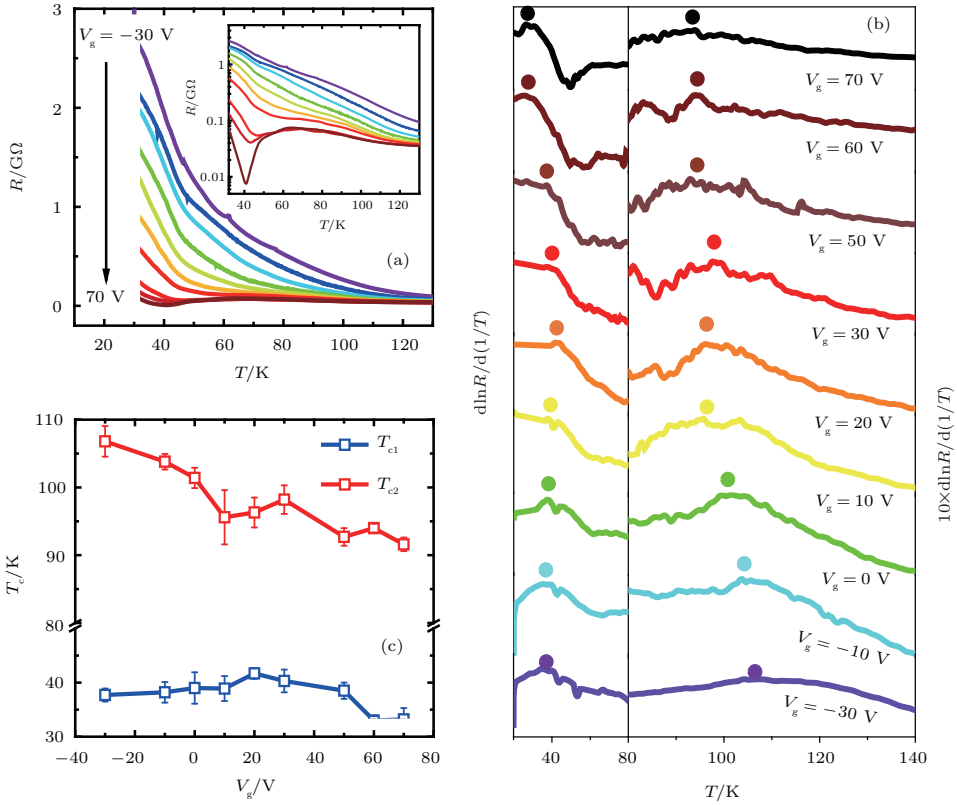


Fig. 3. (color online) Gate-tuned CDW transitions in thin TiS_3 nanoribbon. (a) Temperature-dependent resistance at various gate voltages from −30 V to 70 V except 40 V in a 15-nm device. Inset: the enlarged view of the R–T curve at low temperature regime. (b) Temperature-dependent logarithmic derivative of R–T under different V_g. Right panel, the curves are multiplied by 10 times to display the evolution of CDW phase transition under external gate voltages. (c) The gate voltage dependence of transition temperature T_{c1} and T_{c2}.

Since TiS_3 is a light-sensitive semiconductor, a 633-nm laser (1.94 eV) is used to illuminate the TiS_3 surface as displayed in the inset of Fig. 4(a). The R–T curve shows two phase transitions at 40 K and 85 K without laser illumination (purple curve). The illuminating region of TiS_3 is about 20 μm^2. As the laser intensity gradually increases, the resistance reduces and the phase transition becomes weaker prior to the disappearance under 1.0 μW. Figure 4(c) displays the derivative curves where the threshold intensity is about 1.0 μW and the two peaks come to be completely invisible above this threshold. Though the resistance is monotonically decreased by increasing the laser power, the position of two peaks do not change below 1.0 μW, which can exclude the heating effect. Like the process of light-induced superconductivity suppression,[45,46] laser can destroy the condensate in the distorted region in the CDW state and cause a prompt loss of charge order and equilibration of the electron–lattice system when the absorbed optical energy is higher than the condensation energy (the energy difference between the free energy of the CDW state and the normal state).[47,48] After the excitation, the periodic electron density structure is destroyed and TiS_3 converts to the normal semiconducting state. With a low laser excitation, however, the two phase transitions still exist but are softened with the increasing of the laser intensity, which may be due to the insufficient photons absorbed per unit cell.[49] The low laser excitation can raise the fluctuation but not sufficient to destroy the condensation energy. Figure 4(b) shows the I–V curves under different incident laser intensities at 25 K. The resistance reduces after the laser excitation and the I–V curves become linear under 11-μW laser intensity which indicates that the CDW states and Schottky barrier both disappear. Under 1.0-μW laser intensity, the curve is nonlinear, indicating the Schottky barrier existence while CDW states are destroyed. The quasi-linear I–V curve also shows the suppression of CDW states under laser illumination. Figure 4(d) displays the 532-nm laser condition: under a laser intensity of 0.02 μW, the CDW transitions are substantially weakened and two peaks in the derivative curve disappear (see the inset in Fig. 4(d)). Lower critical intensity of 532-nm laser may attribute to the larger illumination energy. In short, we conclude that the CDW state strongly depends on the excitation energy, reminiscent of superconductivity, where the CDW

pseudo gap state is easily broken by external factors. Below a critical energy, the system needs much more photons to excite the redundant electrons across the gap. Otherwise, the CDW states can still survive.

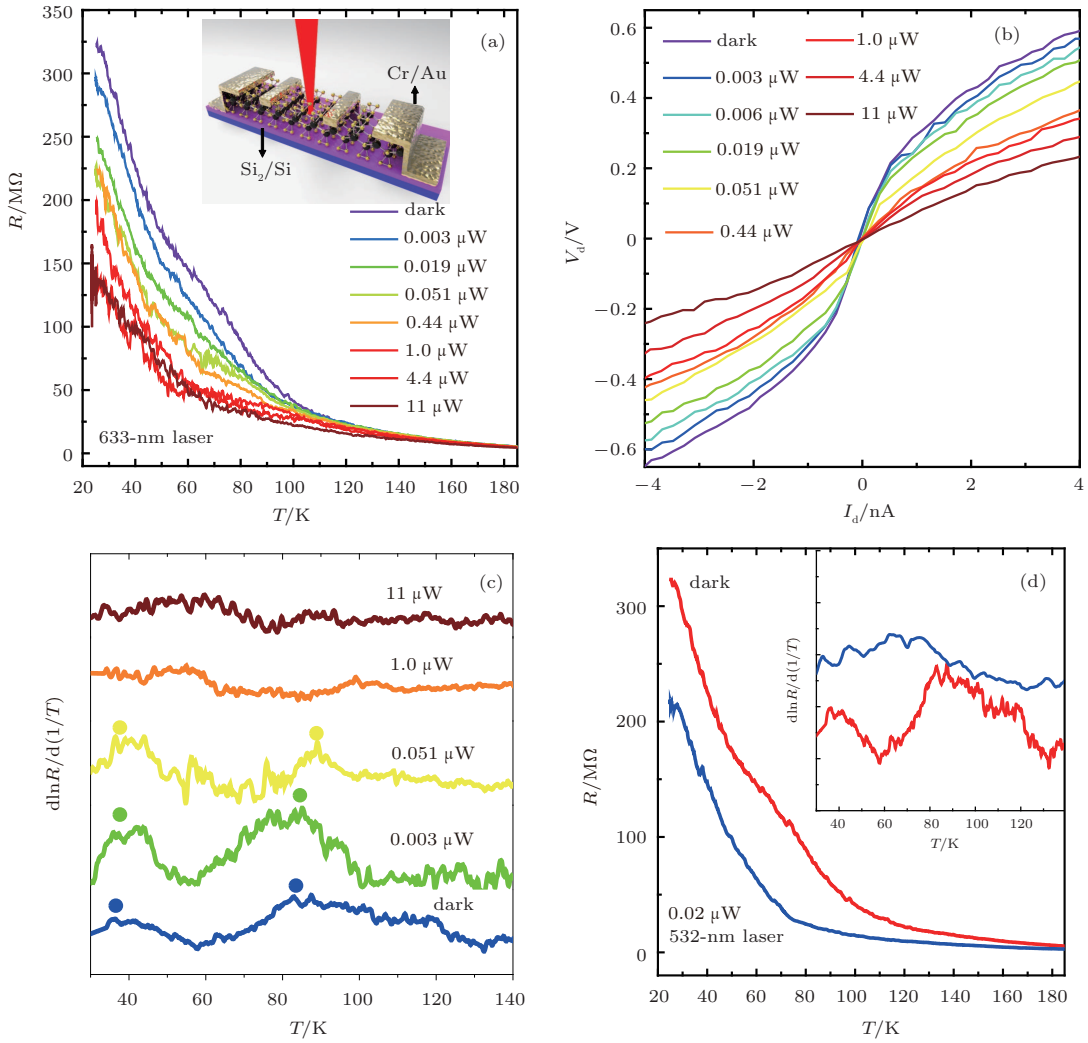


Fig. 4. (color online) Melting of the CDW states by laser. (a) $R-T$ curves under different laser power (0 μW–11 μW). Inset shows a schematic structure of TiS_3 device incident with a 633-nm laser. (b) I_{ds}–V_{ds} curves under different incident laser powers. (c) Temperature-dependent R–T logarithmic derivatives under different laser powers. (d) R–T curves with and without 532-nm laser. Inset displays temperature-dependent R–T logarithmic derivatives.

4. Discussion

Finally, let us briefly compare TiS_3 with previously widely studied CDW in TMDC such as $NbSe_2$. In $NbSe_2$, reducing the dimensionality strengthens the CDW phase and weakens the superconducting phase due to the Fermi surface nesting.[7] In contrast, TiS_3 shows an opposite trend in which thin TiS_3 exhibits a lower transition temperature. The CDW states in TiS_3 are strong anisotropic resulting in the different gate tuning capability because of its robustness to the structural fluctuations. In conclusion, we have performed a systematic study on charge density wave properties in quasi-1D TiS_3 nanoribbons. Two CDW transition temperatures decrease in the thin nanoribbon. The second transition temperature reduces as the increase of the electron doping, while the first transition shows a negligible change. We also observed the light-induced melting of CDW after 633-nm and 532-nm laser illuminations. CDW properties in TMTCs are different from quasi-2D materials such as TMDCs. Our study shows that TiS_3 is a promising CDW material for the study of collective phases in TMTCs and expanding the functionalities for electronic applications like information processing.[50]

Acknowledgement

Part of the sample fabrication was performed at Fudan Nano-fabrication Laboratory.

Appendix A: Supplementary information available

A1. Schottky barrier in thick nanoribbon

Although we use four-probe method to alleviate the effect of contact resistance, Schottky barrier still exists at low

temperatures in two-dimensional devices like MoS_2 as reported before.[31,51] Four-terminal methods are unsuitable if the Schottky behavior occurs between the metallic contact and the sample and the Schottky barrier induces a large contact resistance which may decrease the accuracy of the sample resistance.[32,33] As the nanoribbons are thick enough to be treated as 3D materials, the drain–source current I_{ds} can be defined by 3D thermionic emission equation[34]

$$I_{ds} = AST^2 \exp\left[-\frac{q}{k_B T}\left(\Phi_B - \frac{V_{ds}}{n}\right)\right],$$

where A is the Richardson constant, n is the ideality factor, and V_{ds} is the drain–source voltage.

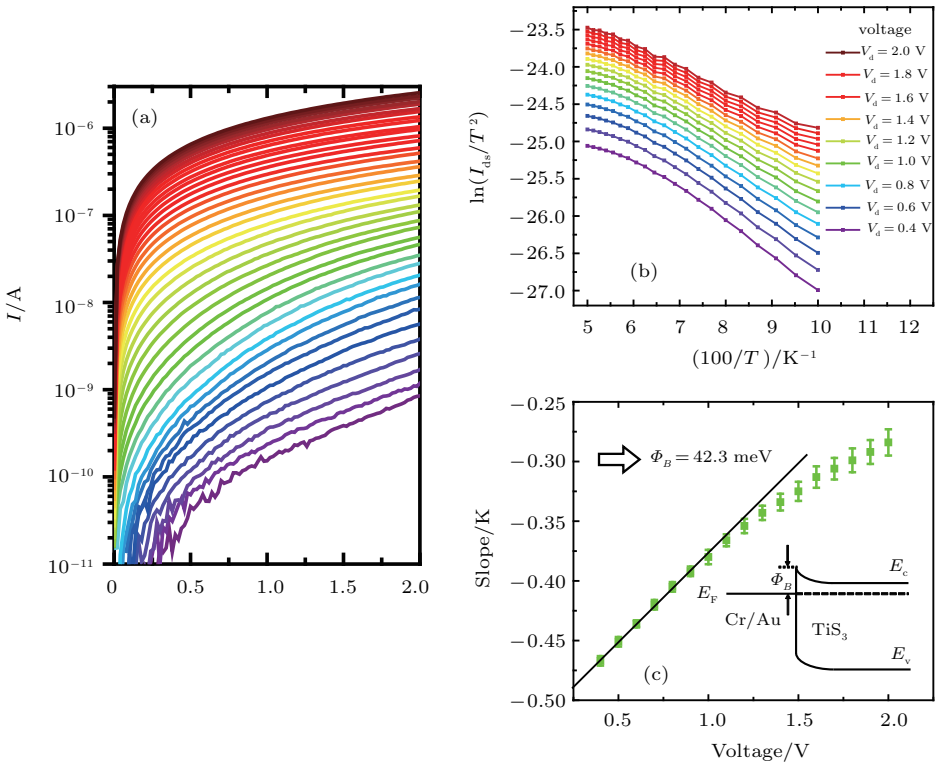


Fig. S1. (color online) Schottky barrier measurements in a thick TiS_3 nanoribbon. (a) I_{ds}–V_{ds} curves on a logarithmic scale from 130 K to 10 K, the red curves correspond to high temperature region, while the blue and purple curves are for low temperature. (b) Arrhenius plot $\ln(I_{ds}/T^2)$ versus $1000/T$ at different voltage V_{ds}. (c) The extraction of Φ_B via the y-intercept value. Each data point here represents the slope obtained from the Arrhenius plot in panel (b) under a specific V_{ds}. The inset shows the band diagram of TiS_3, demonstrating a positive Schottky barrier.

Temperature-dependent I–V measurements were carried out to determine the Schottky barrier height Φ_B as shown in Fig. S1(a). $\ln I_{ds}$ is proportional to V_{ds} from the equation. The curve is linear at $V_{ds} > 0.4$ V on a logarithmic scale. Not enough electrons have overcome the barrier when $V_{ds} < 0.4$ V thus the thermionic emission model is not suitable. Besides, the quasi-1D transport also causes the nonlinear transport that takes a large part in this region. This is also why the fitting in the $V_{ds} > 0.4$ V region is more accurate for the quasi-1D transport. To extract the barrier height, it is common to use Arrhenius plot, $\ln(I_{ds}/T^2)$ against $1000/T$ for various V_{ds} in Fig. S1(b). Fitting the data to each V_{ds}, the slopes with

$$S = -\frac{q}{100k_B}\left(\Phi_b - \frac{V_{ds}}{n}\right)$$

are obtained. Then, we plotted the slopes as a function of V_{ds}. The Schottky barrier height can be extracted from the y-intercept $S_0 = -(q\Phi_B)/(1000k_B) = 42.3$ meV as displayed in Fig. S1(c). The band diagram of the Schottky barrier between Cr/Au and thick TiS_3 is shown in the inset of Fig. S1(c).

A2. FET properties in thin nanoribbon

Figure S2 shows the field-effect-transistor properties of a TiS_3 thin nanoribbon ($\sim$ 15 nm). The gate-dependent conductance G is displayed in Fig. S2(a). Figure S2(b) shows the temperature dependence of mobility. The mobility is extracted from the conductance curves in the 40 V–60 V range of gate voltage V_g using the expression for field-effect mobility $\mu = (dG/dV_g) \times (L_{12}/WC_{ox1})$. The temperature dependence is characterized by a peak at 200 K, below which a decrease of the mobility with the reducing temperature is witnessed. That is caused by the scattering from charged impurities.[52] On the other hand, the mobility decreases as increasing the temperature above 200 K which is related to the electron–phonon scattering.[53] We fit this part of the curve with the generic temperature dependence of the mobility $\mu \sim T^{-\gamma}$, and find the value $\gamma = 1.17$.

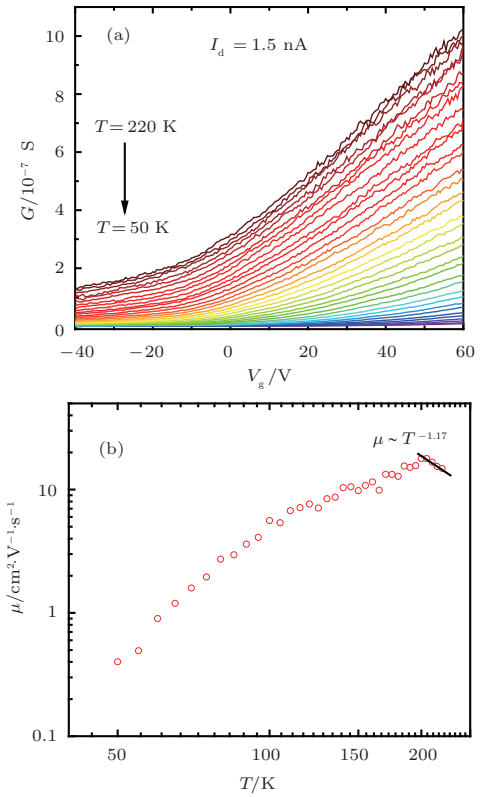


Fig. S2. (color online) FET properties in a thin TiS_3 nanoribbon. (a) Conductance G dependence on the gate voltage from 220 K to 50 K. (b) Temperature dependence of mobility, the region above 200 K is fitted by $\mu \sim T^{-\gamma}$.

A3. Activation energy in thin nanoribbons

Figure S3 shows the field-effect-transistor properties of a TiS_3 thin nanoribbon. The conductance G in the high-temperature regime (8 K$< T <$ 280 K) can be modelled with thermally activated transport: $G = G_0(T)\,\mathrm{e}^{-E_a/k_BT}$, where E_a is the activation energy. However, due to the effect of CDW state below 100 K, we fitted the data above 100 K as shown in Fig. S3(a). Then, we extracted the activation energy E_a and showed its dependence on gate voltage in Fig. S3(b). Examining the deviation of the E_a from the linear trend, which occurs when the barrier tunneling dominates the charge carrier injection,[31] we estimate a Schottky barrier height of $\Phi_B \sim 36$ meV. It is similar to that of the thick sample because the electrical bandgap both in the bulk and few-layer TiS_3 are around 1.2 eV.

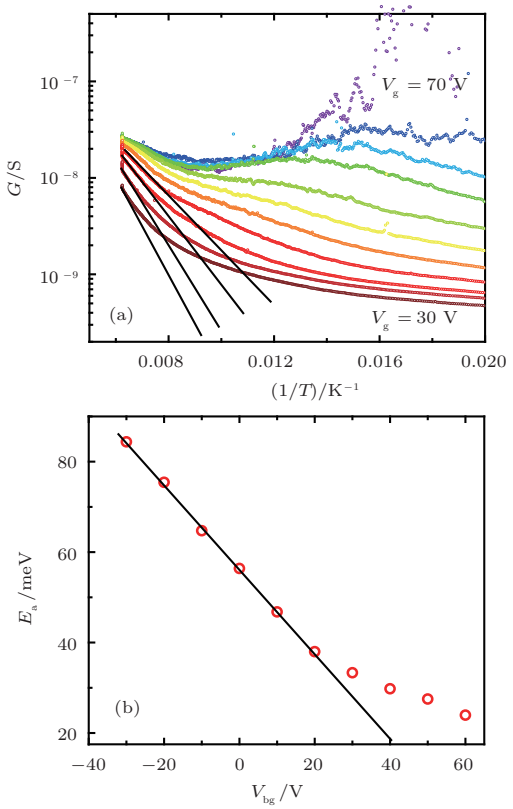
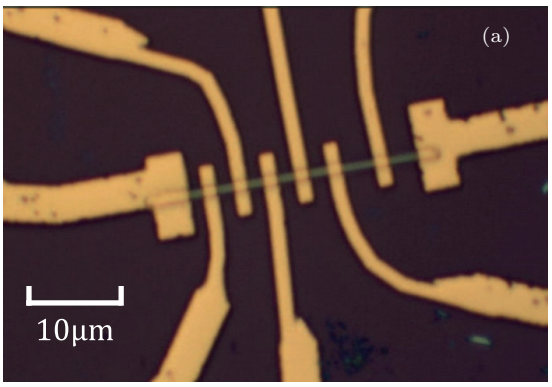


Fig. S3. (color online) Activation energy in a thin TiS_3 nanoribbon. (a) Arrhenius plots of conductance for different gate voltages. Solid lines are linear fits in the high temperature region to extract the activation energy. (b) Gate dependence of activation energies.

A4. Gate-tuned CDW transitions in thick TiS_3 nanoribbon

Figure S4 shows the field-effect-transistor properties of a TiS_3 thick nanoribbon. Even the gate voltage is large at 40 V, the resistance did not change much. It is not easy to tune carrier density in the thick sample, while the two CDW transitions are still evident.



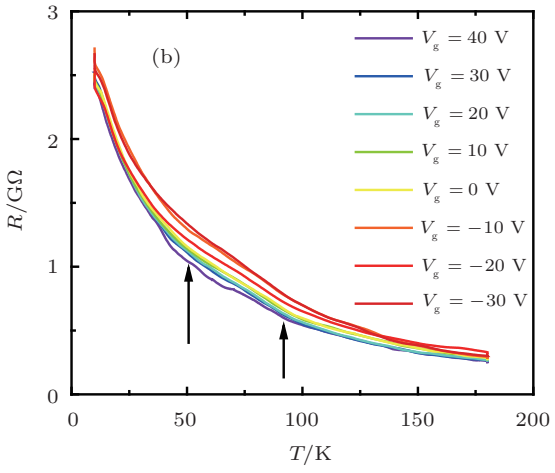


Fig. S4. (color online) Gate-tuned CDW transitions in a thick TiS_3 nanoribbon. (a) An optical microscopy image of a thick TiS_3 FET. (b) Temperature-dependent resistance at various gate voltages. Two CDW transitions are evident.

References

[1] Grüner G 1988 *Rev. Mod. Phys.* **60** 1129
[2] Wilson J A, Di Salvo F and Mahajan S 1975 *Adv. Phys.* **24** 117
[3] Yu Y, Yang F, Lu X F, Yan Y J, Cho Y H, Ma L, Niu X, Kim S, Son Y W and Feng D 2015 *Nat. Nanotechnol.* **10** 270
[4] Chen P, Chan Y H, Fang X Y, Zhang Y, Chou M Y, Mo S K, Hussain Z, Fedorov A V and Chiang T C 2015 *Nat. Commun.* **6** 8943
[5] Ugeda M M, Bradley A J, Zhang Y, Onishi S, Chen Y, Ruan W, Ojeda-Aristizabal C, Ryu H, Edmonds M T and Tsai H Z 2016 *Nat. Phys.* **12** 92
[6] Chatterjee U, Zhao J, Iavarone M, Di Capua R, Castellan J P, Karapetrov G, Malliakas C D, Kanatzidis M G, Claus H, Ruff J P, Weber F, van Wezel J, Campuzano J C, Osborn R, Randeria M, Trivedi N, Norman M R and Rosenkranz S 2015 *Nat. Commun.* **6** 6313
[7] Xi X, Zhao L, Wang Z, Berger H, Forró L, Shan J and Mak K F 2015 *Nat. Nano* **10** 765
[8] Stojchevska L, Vaskivskyi I, Mertelj T, Kusar P, Svetin D, Brazovskii S and Mihailovic D 2014 *Science* **344** 177
[9] Vaskivskyi I, Gospodaric J, Brazovskii S, Svetin D, Sutar P, Goreshnik E, Mihailovic I A, Mertelj T and Mihailovic D 2015 *Sci. Adv.* **1** e1500168
[10] Hodeau J, Marezio M, Roucau C, Ayroles R, Meerschaut A, Rouxel J and Monceau P 1978 *J. Phys. C: Solid State Phys.* **11** 4117
[11] Monceau P, Ong N, Portis A M, Meerschaut A and Rouxel J 1976 *Phys. Rev. Lett.* **37** 602
[12] Moncton D E, Axe J and DiSalvo F 1977 *Phys. Rev. B* **16** 801
[13] Jin Y, Li X and Yang Y 2015 *Phys. Chem. Chem. Phys.* **17** 18665
[14] Yoshida M, Suzuki R, Zhang Y, Nakano M and Iwasa Y 2015 *Sci. Adv.* **1** e1500606
[15] Wilson J 1979 *Phys. Rev. B* **19** 6456
[16] Gruner G 2000 *Density waves in solids* (Westview Press)
[17] errer I, Maciá M, Carcelé V, Ares J and Sáchez C 2012 *Energy Procedia* **22** 48
[18] Dai J and Zeng X C 2015 *Angewandte Chemie* **127** 7682
[19] Island J O, Buscema M, Barawi M, Clamagirand J M, Ares J R, Sánchez C, Ferrer I J, Steele G A, van der Zant H S and Castellanos-Gomez A 2014 *Adv. Opt. Mater.* **2** 641
[20] Wu K, Torun E, Sahin H, Chen B, Fan X, Pant A, Parsons Wright D, Aoki T, Peeters F M, Soignard E and Tongay S 2016 *Nat. Commun.* **7** 12952
[21] Kang J, Sahin H, Ozaydin H D, Senger R T and Peeters F M 2015 *Phys. Rev. B* **92** 075413
[22] Island J O, Biele R, Barawi M, Clamagirand J M, Ares J R, Sanchez C, van der Zant H S, Ferrer I J, D'Agosta R and Castellanos-Gomez A 2015 arXiv: 1510.06889
[23] Gorlova I, Zybtsev S, Pokrovskii V Y, Bolotina N, Verin I and Titov A 2012 *Physica B: Conden. Matter* **407** 1707
[24] Gorlova I, Zybtsev S, Pokrovskii V Y, Bolotina N, Gavrilkin S Y and Tsvetkov A Y 2012 *Physica B: Conden. Matter* **460** 11
[25] Gorlova I, Pokrovskii V Y, Zybtsev S, Titov A and Timofeev V 2010 *J. Exp. and Theor. Phys.* **111** 298
[26] Gorlova I G, Zybtsev S G E and Pokrovskii V Y 2014 *JETP Lett.* **100** 256
[27] Pawbake A S, Island J O, Flores E, Ares J R, Sanchez C, Ferrer I J, Jadkar S R, van der Zant H S, Castellanos-Gomez A and Late D 2015 *ACS Appl. Mater. & Interfaces* **7** 24185
[28] Hsieh P L, Jackson C and Grüer G 1983 *Solid State Commun.* **46** 505
[29] Minakova V, Nasretdinova V and Zaitsev-Zotov S 2015 *Physica B: Conden. Matter* **460** 185
[30] Felser C, Finckh E, Kleinke H, Rocker F and Tremel W 1998 *J. Mater. Chem.* **8** 1787
[31] Radisavljevic B and Kis A 2013 *Nat. Mater.* **12** 815
[32] Hesse E 1982 *IEEE Trans. Instrum. Meas.* **1001** 166
[33] Barnett C, Kryvchenkova O, Wilson L, Maffeis T, Kalna K and Cobley R 2015 *J. Appl. Phys.* **117** 174306
[34] Bhuiyan A, Martinez A and Esteve D 1988 *Thin Solid Films* **161** 93
[35] Slot E, Holst M, Van der Zant H and Zaitsev-Zotov S 2004 *Phys. Rev. Lett.* **93** 176602
[36] Gorlova I G and Pokrovskii V Y 2009 *JETP Lett.* **90** 295
[37] Li L J, O'Farrell E C T, Loh K P, Eda G, Öyilmaz B and Castro Neto A H 2016 *Nature* **529** 185
[38] Imry Y and Ma S K 1975 *Phys. Rev. Lett.* **35** 1399
[39] Sham L and Patton B R 1976 *Phys. Rev. B* **13** 3151
[40] Radisavljevic B, Radenovic A, Brivio J, Giacometti V and Kis A 2011 *Nat. Nanotechnol.* **6** 147
[41] Yang J, Wang W, Liu Y, Du H, Ning W, Zheng G, Jin C, Han Y, Wang N and Yang Z 2014 *Appl. Phys. Lett.* **105** 063109
[42] Goli P, Khan J, Wickramaratne D, Lake R K and Balandin A A 2012 *Nano Lett.* **12** 5941
[43] Morosan E, Zandbergen H, Dennis B, Bos J, Onose Y, Klimczuk T, Ramirez A, Ong N and Cava R 2006 *Nat. Phys.* **2** 544
[44] Adelman T, Zaitsev-Zotov S and Thorne R 1995 *Phys. Rev. Lett.* **74** 5264
[45] Demsar J, Averitt R, Taylor A, Kabanov V, Kang W, Kim H, Choi E and Lee S 2003 *Phys. Rev. Lett.* **91** 267002
[46] Kusar P, Kabanov V V, Demsar J, Mertelj T, Sugai S and Mihailovic D 2008 *Phys. Rev. Lett.* **101** 227001
[47] Tomeljak A, Schaefer H, Stäter D, Beyer M, Biljakovic K and Demsar J 2009 *Phys. Rev. Lett.* **102** 066404
[48] Mör-Vorobeva E, Johnson S L, Beaud P, Staub U, De Souza R, Milne C, Ingold G, Demsar J, Schäer H and Titov A 2011 *Phys. Rev. Lett.* **107** 036403
[49] Ogawa N, Shiraga A, Kondo R, Kagoshima S and Miyano K 2001 *Phys. Rev. Lett.* **87** 256401
[50] Khan J, Nolen C, Teweldebrhan D, Wickramaratne D, Lake R and Balandin A 2012 *Appl. Phys. Lett.* **100** 043109
[51] Wang W, Liu Y, Tang L, Jin Y, Zhao T and Xiu F 2014 *Sci. Rep.* 4
[52] Sze S M and Ng K K 2006 *Physics of semiconductor devices* (John wiley & Sons)
[53] Kaasbjerg K, Thygesen K S and Jacobsen K W 2012 *Phys. Rev. B* **85** 115317